CONDENSED MATTER PHYSICS

A cascade of phase transitions in an orbitally mixed half-filled Landau level

Joseph Falson[1]*, Daniela Tabrea[1], Ding Zhang[2,3], Inti Sodemann[4], Yusuke Kozuka[5,6†], Atsushi Tsukazaki[7], Masashi Kawasaki[5,8], Klaus von Klitzing[1], Jurgen H. Smet[1]*

Half-filled Landau levels host an emergent Fermi liquid that displays instability toward pairing, culminating in a gapped even-denominator fractional quantum Hall ground state. While this pairing may be probed by tuning the polarization of carriers in competing orbital and spin degrees of freedom, sufficiently high quality platforms offering such tunability remain few. We explore the ground states at filling factor ν = 5/2 in ZnO-based two-dimensional electron systems through a forced intersection of opposing spin branches of Landau levels taking quantum numbers N = 1 and 0. We reveal a cascade of phases with distinct magnetotransport features including a gapped phase polarized in the N = 1 level and a compressible phase in N = 0, along with an unexpected Fermi liquid, a second gapped, and a strongly anisotropic nematic-like phase at intermediate polarizations when the levels are near degeneracy. The phase diagram is produced by analyzing the proximity of the intersecting levels and highlights the excellent reproducibility and controllability that ZnO offers for exploring exotic fractionalized electronic phases.

INTRODUCTION

In the presence of strong quantizing perpendicular magnetic fields (B_p), a large class of correlated phases in two-dimensional electron systems (2DES) can be understood as states of weakly interacting composite fermions (CFs); an electron bound to an even number of magnetic vortices (fluxes) (*1*). Of particular significance is the nature of the ground state that forms in half-filled Landau levels (LLs) (*2*–*6*). It is well established that in the half-filled N = 0 LL, a correlated metal forms that can be viewed as a Fermi liquid–like state of CF (*7*). In the N = 1 LL, the Moore-Read (MR) state (*8*), a gapped phase of CF paired in a $p + ip$–wave Bardeen-Cooper-Schrieffer–like fashion, emerges instead. The former is one of the rare examples of a gapless fractionalized phase of matter realized in nature, possibly along with spin liquid candidate materials (*9*), while the latter is one of the few states with Majorana excitations (*10*), along with ^{3}He films, 1D superconducting wires, and spin triplet superconductors like Sr_2RuO_4. However, among these platforms, the MR state is unique in having a truly non-Abelian topological order with fully deconfined point-like non-Abelian quasiparticles, although recent studies have advocated for a closely related state arising in the spin liquid candidate α-$RuCl_3$ (*11*). The potential for demonstrating fault-tolerant quantum computation by braiding these quasi-particle excitations has conjured significant interest around their detection and manipulation (*12*). Insight into the nature of these states may be gained through their study in a regime where LLs are well separated, as well as their fate as a pseudospin degree of freedom is tuned and levels are mixed (*4*–*6*, *13*–*15*). Systems that offer sufficient quality concomitant to experimentally accessible tunability are rare, with bilayer graphene delivering control of the isospin polarization (*16*) of its unique energy spectrum, where the N = 0 and 1 LLs are nearly degenerate (*17*, *18*), and the MgZnO/ZnO-based 2DES through control of the real spin polarization (*4*). The ability to tune these energy levels also provides a vehicle for exploring intermediate polarization regimes, where strong coupling between the pseudospin and real space may result in states with coexisting nematic and ferroelectric-like features (*19*, *20*).

RESULTS

Here, we explore the ground states of the MgZnO/ZnO-based 2DES at filling factor ν = 5/2 across a forced crossing of opposing spin branches of N = 1 and 0 levels, where $\nu = hn/eB_p$, h is the Planck constant, n is the carrier density, and e is the elementary charge. At the neighboring integer filling (ν = 2), it is known that, because of the opposing spin, the transition is a first-order Ising-like spin flop without any intermediate coherence between the two flavors (*21*). It is therefore tempting to speculate that at fractional fillings, one would encounter a similarly simple first-order phase transition between the state that is favored for the respective N = 0 and 1 LLs. However, what we have uncovered is far more complex: At least five distinct phases emerge as charge is transferred between the N = 1 lower spin and the N = 0 upper spin levels. Figure 1 (A to E) illustrates these phases using magnetotransport line traces taken on two samples, *a* and *b*. Each trace is recorded when the sample is oriented at a defined tilt angle (θ) relative to the applied magnetic field, which acts to increase the spin splitting energy and tune the levels toward and ultimately beyond degeneracy, as will be further discussed below. Figure 1A displays transport when the chemical potential (μ_ν) lies in N = 1 and reveals an incompressible phase at ν = 5/2, which we denote as ICP1. Upon increasing θ, this state evolves into a compressible phase (Fig. 1B), denoted as CP1. Then, for a narrow but finite range of θ, a second incompressible phase at ν = 5/2 emerges (ICP2, Fig. 1C taken on sample *b*). This state is supplanted by a strongly anisotropic yet compressible phase (ACP), as per Fig. 1D, which displays the longitudinal resistance taken when the current (I) is sent in two orthogonal crystal directions. Finally, upon full

[1]Max Planck Institute for Solid State Research, Heisenbergstrasse 1, 70569 Stuttgart, Germany. [2]State Key Laboratory of Low-Dimensional Quantum Physics and Department of Physics, Tsinghua University, Beijing 100084, China. [3]Collaborative Innovation Center of Quantum Matter, Beijing 100084, China. [4]Max Planck Institute for the Physics of Complex Systems, 01187 Dresden, Germany. [5]Department of Applied Physics and Quantum-Phase Electronics Center, University of Tokyo, Tokyo 113-8656, Japan. [6]Japan Science and Technology Agency, Precursory Research for Embryonic Science and Technology, Kawaguchi, Saitama 332-0012, Japan. [7]Institute for Materials Research, Tohoku University, Sendai 980-8577, Japan. [8]RIKEN Center for Emergent Matter Science, Wako 351-0198, Japan.
*Corresponding author. Email: j.falson@fkf.mpg.de (J.F.); j.smet@fkf.mpg.de (J.H.S.)
†Present address: Research Center for Magnetic and Spintronic Materials, National Institute for Materials Science, 1-2-1 Sengen, Tsukuba 305-0047, Japan.

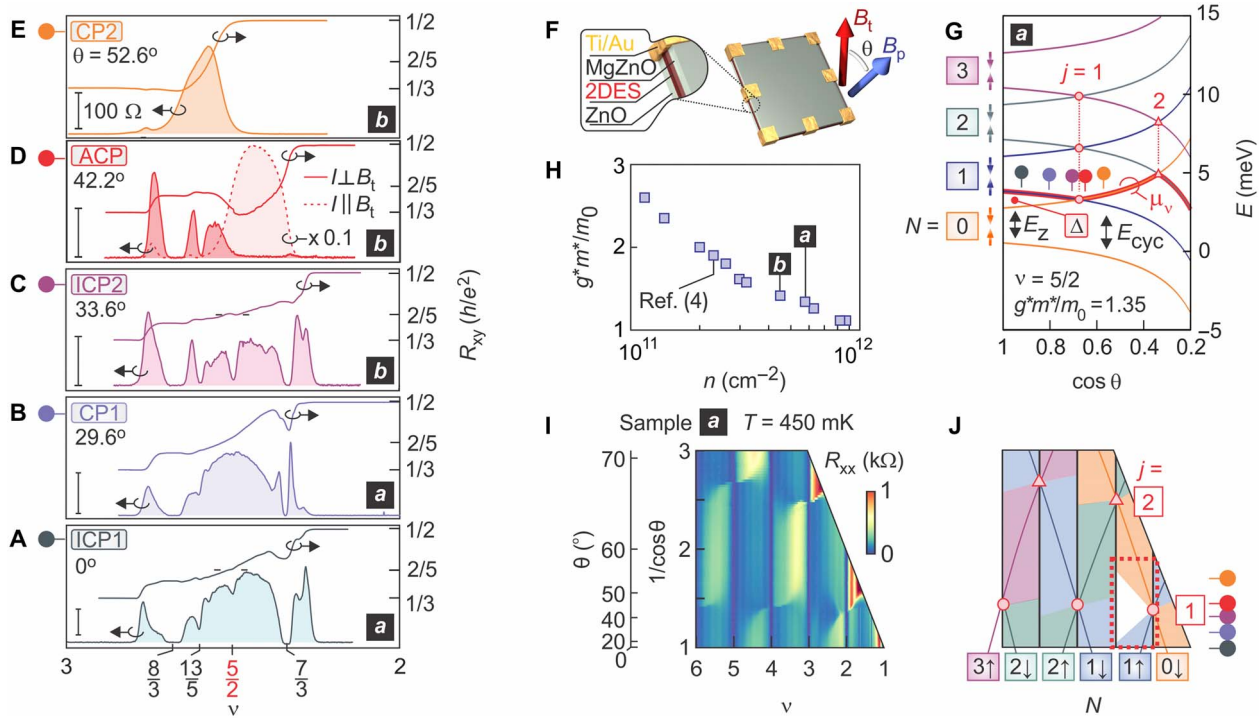

Fig. 1. Overview of correlated phases, samples, and the experimental parameter space. (**A** to **E**) Exemplary magnetotransport sweeps of prominent phases explored in this work. The vertical scale bar corresponds to a longitudinal resistance of 100 ohms. (**F**) Measurement configuration where a MgZnO/ZnO 2DES device is tilted by θ relative to B_t. (**G**) Single-particle energy diagram of spin split LLs, where θ is increased and E_Z is selectively enhanced relative to E_{cyc}, with Δ their energy difference. Opposing spin levels of adjacent LLs cross at the *j*th coincidence position. The chemical potential (μ_ν) is traced as a bold red line for ν = 5/2. (**H**) Spin susceptibility (g^*m^*/m_0) as a function of charge density (*n*). (**I**) T = 450 mK magnetotransport map of sample *a* ($n = 5.8 \times 10^{11}$ cm^{-2}) with (**J**) color coding the corresponding orbital and spin character of partially filled levels and j = 1 and 2 coincidence points.

polarization in $N = 0$ at high θ, the partial filling is rendered compressible (CP2, Fig. 1E). Here, we convey the most poignant experimental findings using two samples but stress that the phase transition cascade is highly reproducible, as summarized at the end of the article. A range of temperatures is used to illustrate certain characteristics: low temperature (T = 20 mK) for ground states and elevated temperatures for charge density wave (CDW) physics (T = 90 mK), hysteretic transport (T = 200 mK), and comprehensive mapping of level crossings (T = 450 mK). Finally, we conclude with a discussion on the possible ground states realized throughout the cascade.

Single-particle level crossings

For a certain sample, we tune between these phases by tilting the MgZnO/ZnO-based 2DES within a magnetic field (Fig. 1F). This is a commonly used technique in 2D systems to selectively enhance the Zeeman energy ($E_Z = g^*\mu_B B_t$, where g^* is the isotropic effective g factor and μ_B is the Bohr magneton) relative to the cyclotron gap ($E_{cyc} = \hbar e B_p/m^*$, where $\hbar$ is the reduced Planck constant and m^* is the effective mass) as the former depends on the total field (B_t) and the latter only on the perpendicular component. Their ratio scales as

$$\frac{E_Z}{E_{cyc}} = \frac{g^*m^*}{2m_0\cos\theta} = j \qquad (1)$$

Here, g^*m^*/m_0 is the spin susceptibility of carriers and governs the energy spacing (Δ) of levels at θ = 0°.

Figure 1G plots the energy diagram of spin split LLs of sample *a* at ν = 5/2 (B_p = 9.6T) as a function of θ using the value of $g^*m^*/m_0 = 1.35$. Following from Eq. 1, E_Z/E_{cyc} may reach an integer value upon increasing θ, which will result in a level crossing, where j is the difference in orbital index of the coinciding levels. Such a crossing will result in a discrete change in orbital character and spin projection of carriers at μ_ν.

In addition to tuning θ, appropriate sample selection is essential for accessing the desired experimental parameter space for probing these crossings. This is due to the renormalization of g^*m^*/m_0 in an interacting 2DES as n is reduced and the magnitude of the Coulomb energy is amplified relative to the zero-field kinetic energy of carriers (*22*). This is a prominent effect in ZnO owing to its relatively small dielectric constant ($\varepsilon = 8.5\varepsilon_0$) and heavy band mass ($m^* = 0.3\ m_0$). In contrast to a density-independent g^*m^*/m_0 predicted for noninteracting electrons, we observe a nearly threefold increase of g^*m^*/m_0 in the ZnO-based heterostructures when reducing n from 10^{12} to 10^{11} cm^{-2}, as shown in Fig. 1H. This can be viewed as the Landau parameters drifting toward the critical value for the appearance of a Stoner-type instability in the dilute limit. Therefore, setting n will determine an initial Δ of the sample, which may then be continuously modified by tuning θ. The single-particle level diagram in Fig. 1G is efficient in capturing the general constellation of level crossings in the experiment, as shown in Fig. 1I for sample *a*. The data are gathered by sweeping B_t at a set θ, which is later used to calculate B_p and ν. Quantum Hall features are seen as dark blue vertical lines. Here, we use an elevated temperature of T = 450 mK to suppress correlated ground states while accentuating the distinct checkerboard

pattern that emerges. We note that the thermal energy at this elevated temperature remains orders of magnitudes smaller than the Coulomb interaction strength, and therefore, we do not encounter significant modifications in the level crossing diagram when increasing T beyond an anticipated smearing of details. Previous studies (*4*, *23*) have shown this checkerboard pattern to be associated with the spin of electrons at μ_ν, with high (low) resistance corresponding to majority (minority) spin ($\sigma = \uparrow,\downarrow$) carriers. The partial filling factor always ends up with high resistance upon full spin polarization, as can be seen at high θ for $\nu < 3$. A comparison with the single-particle energy ladder allows us to assign (N,σ) quantum numbers to the partially filled levels at μ_ν, as shown in Fig. 1J.

Ground states

We now focus on the ground states for $3 > \nu > 2$ filling across the $j = 1$ coincidence between the $1\uparrow$ and $0\downarrow$ levels. This region is framed in the dotted red box in Fig. 1J. We present data from two samples for the following reasons: Sample *a* ($n = 5.8 \times 10^{11}$ cm^{-2}, $g^*m^*/m_0 = 1.35$) has a large intrinsic Δ, which allows us to explore a larger portion of transport in the $N = 1\uparrow$ level but limits the maximum accessible θ at $\nu = 5/2$ because of the experimentally available B field. Sample *b* ($n = 4.4 \times 10^{11}$ cm^{-2}, $g^*m^*/m_0 = 1.48$), however, permits us to observe transport well beyond the first coincidence position, because of its lower n, and in greater detail owing to its higher mobility. Reducing n in sample *b*, however, acts to suppress Δ, which limits the extent to which transport in the $N = 1\uparrow$ level may be observed.

Figure 2A maps the magnetotransport of sample *a* in the (ν-θ) plane at base temperature. Figure 2B tracks the minimum of R_{xx} at $\nu = 5/2$ relative to the surrounding fillings of this map. A positive value of δR_{xx} corresponds to a minimum at $\nu = 5/2$. The ICP1 phase (Fig. 2D) is resolved at low θ and gradually evolves into the CP1 phase by $\theta \sim 25°$. The ICP2 phase appears at $\theta \sim 42.5°$, as per Fig. 2C, and is seen as a spike in δR_{xx} in Fig. 2B. At slightly higher θ, a low-resistance region is resolved and is associated with the ACP, which will be discussed further using Fig. 3.

Figure 3 presents magnetotransport mapping of sample *b* whose intrinsically smaller Δ renders the CP1 phase stable at $\theta = 0°$. Starting from this phase, the same sequence of phases at higher θ is seen. The anisotropic transport is demonstrated by contrasting the data of Fig. 3A and Fig. 3B, where the resistance is taken along two orthogonal crystal directions. The ACP is the ground state for $35° < \theta < 45°$ and $2.3 < \nu < 2.55$. It exhibits easy-axis transport features when $I \perp B_t$, which evidently acts as a symmetry-breaking field as the anisotropic features will reorient by 90° if the projection of B_t is also rotated. This range of θ also exhibits alternative flavors of CDW-like physics: Reentrance of R_{xy} into the integer quantum Hall condition at $\nu = 2$ is seen fanning to higher and lower θ, as marked by the dotted lines in Fig. 3D at $T = 90$ mK. Comparing Fig. 3A and Fig. 3B highlights that the transport is otherwise isotropic away from the ACP phase, and we observe no features associated with coexisting CDW/fractional quantum Hall (FQH) phases (*24*). The higher mobility of sample *b* allows us to plot the activation gaps (Δ_μ) of prominent FQH features as a function of θ (Fig. 3C). The ICP2 phase is realized for a particularly narrow range of θ, beyond which the odd-denominator states of $\nu = 8/3$ and 13/5 display an increase in stability until the system enters the CP2 phase and carriers at μ_ν are polarized in $N = 0\downarrow$.

The crossing at $\nu = 2$ is an Ising transition between two oppositely polarized ferromagnetic states and may be resolved in transport because of the emergence of hysteresis associated with domain formation (*21*). The charge transfer dynamics at fractional filling factors is more elusive as hysteresis is either weak or absent. We can gain a glimpse of

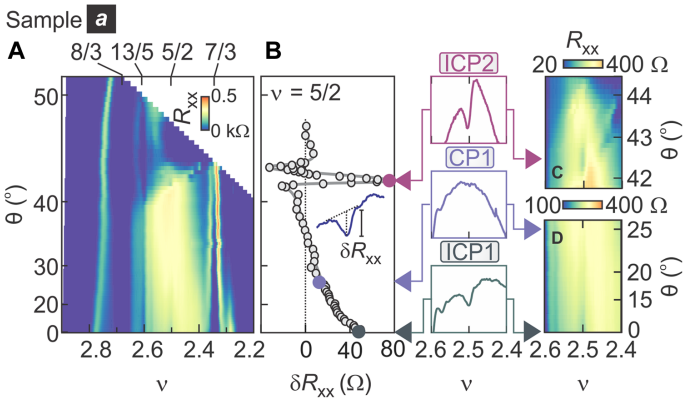

Fig. 2. Ground states of sample *a*. (**A**) $T = 20$ mK magnetotransport map. (**B**) Minimum of resistance (δR_{xx}) at $\nu = 5/2$ relative to surrounding fillings as a function of θ. A positive value indicates a minimum at $\nu = 5/2$, as shown in the inset data trace. Close-up mapping of the (**C**) ICP2 and (**D**) ICP1 and CP1 phases, with boxes displaying magnetotransport traces at the angle indicated by colored arrows. The box height corresponds to Δ200 ohms.

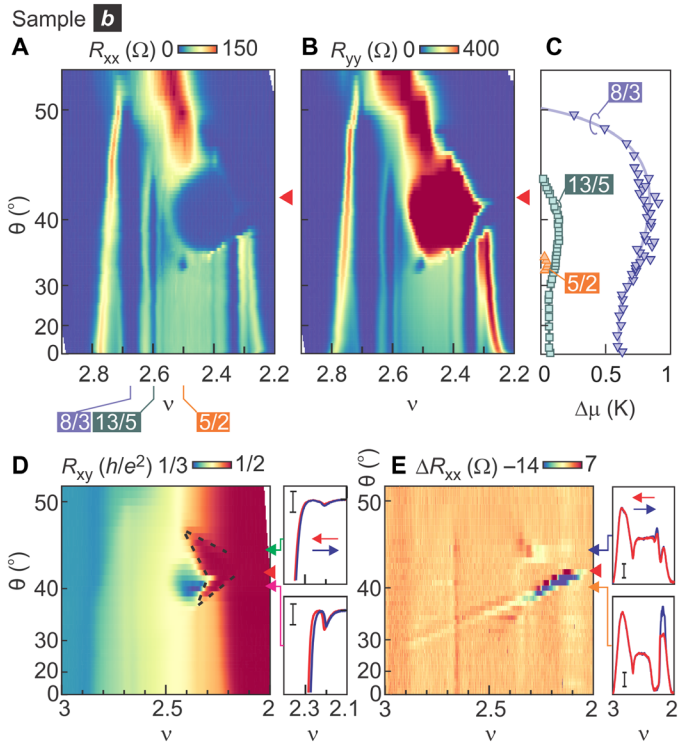

Fig. 3. Ground states and hysteresis of sample *b*. (**A** and **B**) Magnetotransport maps ($T = 20$ mK) for two orthogonal crystal directions, with R_{xx} associated with $I \perp B_t$ and R_{yy} with $I \| B_t$. (**C**) Activation energy Δ_μ of prominent FQH states. (**D**) Isotropic reentrant integer quantum Hall features at $T = 90$ mK: mapping of R_{xy} with reentrant integer quantum Hall features of $\nu = 2$ framed by dotted lines. The subpanels identify their hysteretic behavior, with the scale bar equaling 0.1[h/e^2]. (**E**) Hysteresis at $T = 200$ mK: mapping of ΔR_{xx}. Individual traces with B-sweep direction–dependent transport are shown for discrete angles in the subpanels. The scale bar corresponds to an R_{xx} of 10 ohms. Red triangles indicate the $j = 1|_{\nu=2}$ coincidence position.

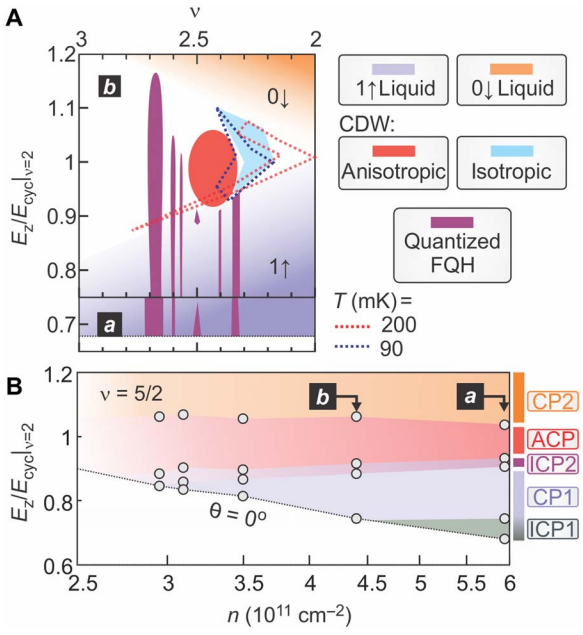

Fig. 4. Phase diagram of ground states. (**A**) Map of the ground states in the (ν-E_Z/E_{cyc}) plane through the transitions from N = 1↑ (light purple) to 0↓ (orange) orbital character. The range of FQH features is shown as purple, with the anisotropic CDW-like phase shaded red and isotropic reentrant phases shaded light blue. The range of hysteretic features identified in transport maps is shown as dotted lines for T = 200 mK (red) and 90 mK (blue). (**B**) Summary of the transitions at ν = 5/2 in terms of $E_Z/E_{cyc}|_{j=2}$ as a function of n, as per Eq. 1.

this by inspecting the hysteretic component of transport at an elevated temperature of T = 200 mK, as shown in Fig. 3E. These data are constructed by taking two transport maps, one composed of only down-sweep and the other only up-sweep B-field data, with the difference (ΔR_{xx}) being displayed. Strong hysteretic features are observed close to ν = 2 and is evidence of a first-order transition associated with the exchange-corrected single-particle level crossing at j = 1 (red arrow, see the Supplementary Materials) (*25*). These markedly weaken at fractional fillings of ν > 2.3. We also note the weaker features in the subpanels of Fig. 3 (D and E), which emerge in the vicinity of reentrant features at both higher and lower θ relative to the j = 1 crossing position.

Phase diagram

Figure 4 summarizes the phase diagram of competing ground states. Figure 4A is a composite representation of the extent of the ground states in the (ν-E_Z/E_{cyc}) plane for samples *a* and *b*, including FQH (dark purple) features, 1↑ (light purple) and 0↓ (orange) polarized liquids, and anisotropic (red) and isotropic (blue) CDW-like phases. For the sake of constructing this diagram, we determine E_Z/E_{cyc} using the g^*m^*/m_0 quantized at $j = 1|_{\nu=2}$ and using Eq. 1. This representation allows us to define a single-particle energy scale for the sake of discussion and comparison (see the Supplementary Materials). Extrapolating the hysteretic features observed near ν = 2 at T = 200 mK (red; Fig. 4A) and 90 mK (blue; see the Supplementary Materials) permits us to illustrate a range in which the 2DES is depolarized and has mixed N = 0 and 1 character. The ν = 8/3 and 13/5 states do not close their charge gap across the lower bound of this mixed regime (Fig. 3C). Moreover, the ICP2 and ACP phases emerge only within these bounds. These observations support our hypothesis that the charge transfer at fractional fillings is unique and gradually occurs over a large range of θ rather than at a single discrete angle. Figure 4B highlights the reproducibility of the phase diagram by plotting the cascade as a function of n; the E_Z/E_{cyc} ratio emerges as the determining factor of the stability of ground states for all samples. It also conveys why these phases evaded detection in previous works (*4*): The sample investigated ($n = 2.3 \times 10^{11}$ cm^{-2}, g^*m^*/m_0 = 1.9) put the majority of phases out of experimental reach because of its intrinsic E_Z/E_{cyc} ratio of approximately 0.95.

DISCUSSION

Henceforth, we discuss candidate states for the observed phases by using the CF picture at ν = 5/2. We will construct states by adding holes to the neighboring integer quantum Hall state at ν = 3, and thus, we write $\nu = 3 - (\nu_{h0} + \nu_{h1})$, with $\nu_{h0} + \nu_{h1} = 1/2$ the partial hole fillings of the $N = 0(\downarrow)/1(\uparrow)$ components. Because of the strong Coulomb interaction strength and small cyclotron gaps in our system, we expect strong inter-LL excitations, as the LL mixing parameter ($\kappa = E_{Coulomb}/E_{cyc}$) exceeds 5 for all samples (see fig. S3). While difficult to capture systematically in the experiment, the mixing between levels can manifest as a suppression of activation gaps of ground states and also more subtly as a result of imposing symmetry-breaking terms on particle-hole invariant phases, which would ultimately determine the ground of the even-denominator FQH phases present in the experiment (*26*–*30*).

When Δ is large (n is large), the ICP1 phase is likely the MR state (*31*) for $\nu_{h0} = 0$ and $\nu_{h1} = 1/2$. An interesting possibility as the crossing is approached is a mixed state known as the Z_2 exciton metal with the coexistence of pairing of the N = 1 component and a composite Fermi liquid in the N = 0 component (*5*, *13*, *14*). In the case of bilayer graphene, valley is a conserved quantum number across the transition, while in ZnO it is the electron spin. This state would have $R_{xx} \to 0$ and $R_{xy}[h/e^2] = 2/5$ as $T \to 0$ (see the Supplementary Materials), and hence is not ruled out by our observations, although measurement of the spin polarization will be needed to confirm its presence.

The CP2 phase naturally corresponds to $\nu_{h0} = 1/2$; $\nu_{h1} = 0$. Surprisingly, odd-denominator FQH physics is entirely absent in this regime, despite the N = 0 orbital character. We attribute this to the reduced screening of the polarized state that stems from an increased Pauli blocking of virtual transitions. This reduced screening enhances the effective disorder potential, degrading the quality of the odd-denominator FQH features and increasing the width of the ν = 2 plateau.

The physics of CP1 is subtle as it emerges in the vicinity of the level crossing of $N = 0\downarrow$ and $1\uparrow$ as Δ is made small. Accordingly, we speculate that this phase corresponds to a state with two Fermi surfaces [$(\nu_{h0}; \nu_{h1}) \neq 0$]. States with two composite Fermi surfaces are known to be energetically favored in the case of spinful N = 0 LL with small Zeeman splitting (*32*, *33*). Therefore, it is not unreasonable that partially polarized two-component Fermi sea states might arise in our case of a spinful two-component orbitally mixed system [(*5*, *13*, *14*) and a further discussion in the Supplementary Materials].

The nature of the ICP2 phase constitutes another intriguing puzzle. Such a phase has not been observed in the experimental works on crossing of valley-polarized levels in bilayer graphene (*5*, *6*) or in associated theoretical works (*13*, *14*). One possibility is a paired MR state, which has been found to exhibit enhanced stability near level crossings of subbands in GaAs (*34*). Another alternative is that ICP2 is a paired state distinct from the MR state. A natural candidate would be the Halperin-331 state, which is two-component and could therefore be favored near the level crossing (*8*, *35*) yet would be composed of components with differing spin and orbital character.

Finally, we discuss the CDW-like physics that emerges between ICP2 and CP2. It is important to emphasize that the ACP phase is not restricted to ν = 5/2 but pervades a large portion of the filling fraction range. No analogous feature was observed in the previous reports in bilayer graphene (*5*, *6*). A natural candidate is the stripe phase seen in higher LLs ($N \geq 2$) in GaAs (*36*, *37*). There, the FQH effect is expelled as CDW physics becomes energetically favorable. Similar features can be induced in $N = 1$ as the MR state is in close competition with a stripe phase (*38*–*41*). What makes the ACP state in this work unexpected is its stabilization near the level crossing as $N = 0$ character is increased, as evidenced by the increase in activation energy of odd-denominator states at ν = 8/3 and 13/5 for the same range of θ (Fig. 3C). The anisotropy is also notably askew toward low ν, where isotropic reentrant features additionally emerge. One possibility is strong mixing between higher LLs stabilizing a stripe phase. A more exotic alternative scenario to conventional stripes is that ACP corresponds to a coherent state between $N = 0\downarrow$ and $1\uparrow$ levels. As these orbitals carry different angular momenta, a coherent superposition would break inversion and rotation symmetries. This would endow the state with nematic and ferroelectric characteristics, explaining its anisotropic nature. In addition, the opposite spin would render the state with a finite magnetization in the plane orthogonal to the spin polarization axis dictated by E_Z. While proposals for related ferroelectric states in bilayer graphene have been made at integer fillings (*19*), we are not aware of studies addressing their energetic feasibility for fractionally filled levels. We hope that our results motivate future numerical and experimental studies of these possibilities.

In summary, the exotic sequence of phases observed at the crossing of the $N = 0$ and 1 LLs is consistent with a gradual and complex depolarization sequence of the orbital character, in contrast to the expectations of a simple spin-flop first-order transition. In addition to LL-polarized states, the unexpected observation of incompressible and anisotropic phases in the orbitally mixed regime opens important questions concerning their nature and the possibility of novel interlayer coherence arising at fractional filling factors in a system with strong LL mixing.

MATERIALS AND METHODS

The $Mg_xZn_{1-x}O$/ZnO heterostructures were grown using ozone molecular beam epitaxy (*42*). The $Mg_xZn_{1-x}O$ layer was typically 500 nm and was deposited on top of a 500-nm ZnO homoepitaxial layer grown on highly conducting Zn-polar Tokyo Denpa ZnO single-crystal substrates. Samples *a* ($n = 5.8 \times 10^{11}$ cm^{-2}, $x \sim 0.04$, $g^*m^*/m_0 = 1.35$) and *b* ($n = 4.4 \times 10^{11}$ cm^{-2}, $x \sim 0.03$, $g^*m^*/m_0 = 1.48$) have electron mobilities of 190,000 and 350,000 cm^2/Vs. Measurements were performed in a top-loading-into-the-mixture ($T_{base} \sim 20$ mK) dilution refrigerator equipped with a rotation stage. Low-frequency AC lock-in techniques were used to gather resistance data.

SUPPLEMENTARY MATERIALS

Supplementary material for this article is available at http://advances.sciencemag.org/cgi/content/full/4/9/eaat8742/DC1

REFERENCES AND NOTES

1. J. K. Jain, *Composite Fermions* (Cambridge Univ. Press, 2007).
2. R. Willett, J. P. Eisenstein, H. L. Störmer, D. C. Tsui, A. C. Gossard, J. H. English, Observation of an even-denominator quantum number in the fractional quantum Hall effect. *Phys. Rev. Lett.* **59**, 1776 (1987).
3. D.-K. Ki, V. I. Fal'ko, D. A. Abanin, A. F. Morpurgo, Observation of even denominator fractional quantum Hall effect in suspended bilayer graphene. *Nano Lett.* **14**, 2135–2139 (2014).
4. J. Falson, D. Maryenko, B. Friess, D. Zhang, Y. Kozuka, A. Tsukazaki, J. H. Smet, M. Kawasaki, Even-denominator fractional quantum Hall physics in ZnO. *Nat. Phys.* **11**, 347–351 (2015).
5. A. A. Zibrov, C. Kometter, H. Zhou, E. M. Spanton, T. Taniguchi, K. Watanabe, M. P. Zaletel, A. F. Young, Tunable interacting composite fermion phases in a half-filled bilayer-graphene Landau level. *Nature* **549**, 360–364 (2017).
6. J. I. A. Li, C. Tan, S. Chen, Y. Zeng, T. Taniguchi, K. Watanabe, J. Hone, C. R. Dean, Even-denominator fractional quantum Hall states in bilayer graphene. *Science* **358**, 648–652 (2017).
7. B. I. Halperin, P. A. Lee, N. Read, Theory of the half-filled Landau level. *Phys. Rev. B* **47**, 7312 (1993).
8. N. Read D. Green, Paired states of fermions in two dimensions with breaking of parity and time-reversal symmetries and the fractional quantum Hall effect. *Phys. Rev. B* **61**, 10267 (2000).
9. Y. Zhou, K. Kanoda, T.-K. Ng, Quantum spin liquid states. *Rev. Mod. Phys.* **89**, 025003 (2017).
10. J. Alicea, New directions in the pursuit of Majorana fermions in solid state systems. *Rep. Prog. Phys.* **75**, 076501 (2012).
11. Y. Kasahara, K. Sugii, T. Ohnishi, M. Shimozawa, M. Yamashita, N. Kurita, H. Tanaka, J. Nasu, Y. Motome, T. Shibauchi, Y. Matsuda, Unusual thermal Hall effect in a Kitaev spin liquid candidate α–$RuCl_3$. *Phys. Rev. Lett.* **120**, 217205 (2018).
12. C. Nayak, S. H. Simon, A. Stern, M. Freedman, S. Das Sarma, Non-Abelian anyons and topological quantum computation. *Rev. Mod. Phys.* **80**, 1083 (2008).
13. M. Barkeshli, C. Nayak, Z. Papić, A. Young, M. Zaletel, Topological exciton Fermi surfaces in two-component fractional quantized Hall insulators. *Phys. Rev. Lett.* **121**, 026603 (2018).
14. M. P. Zaletel, S. Geraedts, Z. Papić, E. H. Rezayi, Evidence for a topological "exciton Fermi sea" in bilayer graphene. *Phys. Rev. B* **98**, 045113 (2018).
15. Y. Liu, M. A. Mueed, M. Shafayat Hossain, S. Hasdermir, L. N. Pfeiffer, K. W. West, K. W. Baldwin, M. Shayegan, Morphing of two-dimensional hole systems at ν = 3/2 in parallel magnetic fields: Compressible, stripe, and fractional quantum Hall phases. *Phys. Rev. B* **94**, 155312 (2016).
16. B. M. Hunt, J. I. A. Li, A. A. Zibrov, L. Wang, T. Taniguchi, K. Watanabe, J. Hone, C. R. Dean, M. Zaletel, R. C. Ashoori, A. F. Young, Direct measurement of discrete valley and orbital quantum numbers in bilayer graphene. *Nat. Commun.* **8**, 948 (2017).
17. K. S. Novoselov, E. McCann, S. V. Morozov, V. I. Fal'ko, M. I. Katsnelson, U. Zeitler, D. Jiang, F. Schedin, A. K. Geim, Unconventional quantum Hall effect and Berry's phase of 2π in bilayer graphene. *Nat. Phys.* **2**, 177–180 (2006).
18. E. McCann, V. I. Fal'ko, Landau-level degeneracy and quantum Hall effect in a graphite bilayer. *Phys. Rev. Lett.* **96**, 086805 (2006).
19. R. Côté, J. Lambert, Y. Barlas, A. H. MacDonald, Orbital order in bilayer graphene at filling factor ν = −1. *Phys. Rev. B* **82**, 035445 (2010).
20. R. Côté, J. P. Fouquet, W. Luo, Biased bilayer graphene as a helical quantum Hall ferromagnet. *Phys. Rev. B* **84**, 235301 (2011).
21. E. P. De Poortere, E. Tutuc, S. J. Papadakis, M. Shayegan, Resistance spikes at transitions between Quantum Hall ferromagnets. *Science* **290**, 1546–1549 (2000).
22. T. Gokmen, M. Padmanabhan, M. Shayegan, Contrast between spin and valley degrees of freedom. *Phys. Rev. B* **81**, 235305 (2010).
23. D. Maryenko, J. Falson, Y. Kozuka, A. Tsukazaki, M. Kawasaki, Polarization-dependent Landau level crossing in a two-dimensional electron system in a MgZnO/ZnO heterostructure. *Phys. Rev. B* **90**, 245303 (2014).
24. Y. Liu, S. Hasdemir, M. Shayegan, L. N. Pfeiffer, K. W. West, K. W. Baldwin, Evidence for a ν = 5/2 fractional quantum Hall nematic state in parallel magnetic fields. *Phys. Rev. B* **88**, 035307 (2013).

25. G. Giuliani, G. Vignale, *Quantum Theory of the Electron Liquid* (Cambridge Univ. Press, 2005).
26. S. H. Simon, E. H. Rezayi, Landau level mixing in the perturbative limit. *Phys. Rev. B* **87**, 155426 (2013).
27. I. Sodemann, A. H. MacDonald, Landau level mixing and the fractional quantum Hall effect. *Phys. Rev. B* **87**, 245425 (2013).
28. M. R. Peterson, C. Nayak, More realistic Hamiltonians for the fractional quantum Hall regime in GaAs and graphene. *Phys. Rev. B* **87**, 245129 (2013).
29. W. Luo, T. Chakraborty, Missing fractional quantum Hall states in ZnO. *Phys. Rev. B* **93**, 161103(R) (2016).
30. W. Luo, T. Chakraborty, Pfaffian state in an electron gas with small Landau level gaps. *Phys. Rev. B* **96**, 081108(R) (2017).
31. G. Moore N. Read, Nonabelions in the fractional quantum Hall effect. *Nucl. Phys. B* **360**, 362–396 (1991).
32. I. V. Kukushkin, K. V. Klitzing, K. Eberl, Spin polarization of composite fermions: Measurements of the Fermi energy. *Phys. Rev. Lett.* **82**, 3665 (1999).
33. L. Tiemann, G. Gamez, N. Kumada, K. Muraki, Unraveling the spin polarization of the $\nu = 5/2$ fractional quantum Hall state. *Science* **335**, 828–831 (2012).
34. Y. Liu, D. Kamburov, M. Shayegan, L. N. Pfeiffer, K. W. West, K. W. Baldwin, Anomalous robustness of the $\nu = 5/2$ fractional quantum Hall state near a sharp phase boundary. *Phys. Rev. Lett.* **107**, 176805 (2011).
35. Y. Liu, S. Hasdemir, D. Kamburov, A. L. Graninger, M. Shayegan, L. N. Pfeiffer, K. W. West, K. W. Baldwin, R. Winkler, Even-denominator fractional quantum Hall effect at a Landau level crossing. *Phys. Rev. B* **89**, 165313 (2014).
36. A. A. Koulakov, M. M. Fogler, B. I. Shklovskii, Charge density wave in two-dimensional electron liquid in weak magnetic field. *Phys. Rev. Lett.* **76**, 499–502 (1996).
37. M. P. Lilly, K. B. Cooper, J. P. Eisenstein, L. N. Pfeiffer, K. W. West, Evidence for an anisotropic state of two-dimensional electrons in high Landau levels. *Phys. Rev. Lett.* **82**, 394–397 (1999).
38. M. P. Lilly, K. B. Cooper, J. P. Eisenstein, L. N. Pfeiffer, K. W. West, Anisotropic states of two-dimensional electron systems in high Landau levels: Effect of an in-plane magnetic field. *Phys. Rev. Lett.* **83**, 824–827 (1999).
39. W. Pan, R. R. Du, H. L. Stormer, D. C. Tsui, L. N. Pfeiffer, K. W. Baldwin, K. W. West, Strongly anisotropic electronic transport at Landau level filling factor $\nu = 9/2$ and $\nu = 5/2$ under a tilted magnetic field. *Phys. Rev. Lett.* **83**, 820–823 (1999).
40. E. H. Rezayi, F. D. M. Haldane, Incompressible paired Hall state, stripe order, and the composite fermion liquid phase in half-filled Landau levels. *Phys. Rev. Lett.* **84**, 4685–4688 (2000).
41. N. Samkharadze, K. A. Schreiber, G. C. Gardner, M. J. Manfra, E. Fradkin, G. A. Csáthy, Observation of a transition from a topologically ordered to a spontaneously broken symmetry phase. *Nat. Phys.* **12**, 191–195 (2016).
42. J. Falson, M. Kawasaki, A review of the quantum Hall effects in MgZnO/ZnO heterostructures. *Rep. Prog. Phys.* **81**, 056501 (2018).
43. V. V. Solovyev, A. B. Van'kov, I. V. Kukushkin, J. Falson, D. Zhang, D. Maryenko, Y. Kozuka, A. Tsukazaki, J. H. Smet, M. Kawasaki, Optical probing of MgZnO/ZnO heterointerface confinement potential energy levels. *Appl. Phys. Lett.* **106**, 082102 (2015).
44. R. R. Du, A. S. Yeh, H. L. Stormer, D. C. Tsui, L. N. Pfeiffer, K. W. West, Fractional quantum Hall effect around $\nu = 3/2$: Composite fermions with a spin. *Phys. Rev. Lett.* **75**, 3926–3929 (1995).
45. M. Barkeshli, J. McGreevy, Continuous transitions between composite Fermi liquid and Landau Fermi liquid: A route to fractionalized Mott insulators. *Phys. Rev. B* **86**, 075136 (2012).
46. L. B. Ioffe, A. I. Larkin, Gapless fermions and gauge fields in dielectrics. *Phys. Rev. B* **39**, 8988 (1989).

Acknowledgments: We appreciate discussions with M. Barkeshli, H. Boschker, B. Feldman, Y. Liu, and M. Zudov. **Funding:** We acknowledge the financial support of Japan Science and Technology Agency (JST) Core Research for Evolutional Science and Technology grant number JPMJCR16F1. J.F. acknowledges the Max Planck–University of British Columbia–University of Tokyo Center for Quantum Materials and the Deutsche Forschungsgemeinschaft (FA 1392/2-1). Y.K. acknowledges JST Precursory Research for Embryonic Science and Technology grant number JPMJPR1763. **Author contributions:** J.F., D.T., and D.Z. gathered the transport data. J.F. grew the samples with assistance from Y.K., A.T., and M.K. J.F. and I.S. wrote the manuscript following discussion and input from all authors. **Competing interests:** The authors declare that they have no competing interests. **Data and materials availability:** All data needed to evaluate the conclusions in the paper are present in the paper and/or the Supplementary Materials. Additional data related to this paper may be requested from the authors.

Submitted 16 April 2018
Accepted 2 August 2018
Published 14 September 2018
10.1126/sciadv.aat8742

Citation: J. Falson, D. Tabrea, D. Zhang, I. Sodemann, Y. Kozuka, A. Tsukazaki, M. Kawasaki, K. von Klitzing, J. H. Smet, A cascade of phase transitions in an orbitally mixed half-filled Landau level. *Sci. Adv.* **4**, eaat8742 (2018).